Lack of evidence for one-photon coherent control of the primary photoisomerisation in retinal proteins

M. Liebel[1] and P. Kukura*

Physical and Theoretical Chemistry Laboratory, University of Oxford, South Parks Road, OX1 3QZ Oxford, UK.

[1]Current address: ICFO-Institut de Ciències Fotòniques, The Barcelona Institute of Science and Technology, 08860 Castelldefels, Barcelona, Spain

*philipp.kukura@chem.ox.ac.uk

The concept of shaping electric fields to coherently steer light induced processes has fascinated scientists for decades. Despite early theoretical considerations ruling out one-photon coherent control, several experimental studies have reported excitation field shape dependent molecular responses in the weak-field limit. These observations were largely attributed to the presence of rapid decay channels, but experimental verification is lacking. Here, we rigorously test this hypothesis by investigating the degree of achievable control over the photoisomerisation of the retinal protonated Schiff base in bacteriorhodopsin, isorhodopsin and rhodopsin, all of which exhibit similar chromophores but different isomerisation yields and excited state lifetimes. Irrespective of the system studied, we find no evidence for dissipation-dependent behaviour, nor for any coherent control in the strict one photon limit. Our results raise the question to which extent a photochemical process at ambient condition can be controlled at the amplitude level and how the underlying molecular potential energy surfaces and dynamics may influence this controllability.

Coherent control (CC) [1–8] aims to modify the outcome of a photochemical processes with precisely tailored electric fields. In a pump-dump CC experiment [1], a pump pulse populates an excited electronic state, which is subsequently transferred into the desired photoproduct state by a time-delayed dump pulse. This scenario necessarily requires the interaction of the system with more than one photon and is therefore often referred to as high-field CC [7]. Under weak-field excitation conditions, where only one photon interacts with each molecule, closed quantum systems have originally been predicted to be insensitive to the shape of the incident electric field [9]. This view has been revised for operators representing a control target that does not commute with the system Hamiltonian and for dissipative systems even if the relevant operators do commute [10]. For the latter, the degree of control has been predicted to scale with the relative timescales of environmentally-assisted dissipation and employed pulse durations not only in simple systems [11], but also in more realistic representations [12] of the seminal experimental results on the photoisomerisation of the retinal protonated Schiff base [13]. Taken together, these theoretical studies support the notion that a specifically shaped excitation field generates a complex vibronic wavepacket, which evolves differently to a wavepacket generated by an electric field with a flat phase (Figure 1a) [2]. Bath-induced collapse of the coherence then acts in a similar way to the dump pulse in a high-field CC experiment [1,14]. Weak-field control thereby becomes feasible even though only one photon is involved in the overall process [10,11].

Given the potential of CC to further the understanding of ultrafast processes it is surprising that the initial experimental reports of weak-field CC [13,15,16] have almost exclusively been followed up theoretically. The lack of experimental studies is most likely a consequence of the technical hurdles associated with weak-field CC experiments and the lack of suitable molecular systems with appropriately tuneable reactive properties. To address these shortcomings, we report a self-referenced approach to weak-field CC experiments on retinal protonated Schiff base chromophores embedded in different protein pockets. We employ the three opsin proteins bacteriorhodopsin (bR), rhodopsin (rho) and isorhodopsin (isorho) with the respective reactant chromophore being in the all-*trans*, 11-*cis* and 9-*cis* configuration, respectively [17–19]. Both bR and rho exhibit approximately the same photoisomerisation quantum yield of ~65% but the latter isomerises almost ten times times faster (600 fs vs ~70 fs excited state lifetime) [20,21]. Rho and isorho form the same all-*trans* photoproduct, bathorhodopsin, and the retinal protonated Schiff base chromophore is embedded in an identical opsin environment. The reaction speed (~70 vs 200 fs) and its efficiency (65 vs 22 % quantum yield), however, differ considerably [18,21,22]. As all of these chromophores undergo an ultrafast photoisomerisation, they should in principle be controllable in the weak-field limit according to both proposed criteria for weak-field control [10]. Furthermore, a recent theoretical study

suggested that isorho could be an ideal CC candidate [19]. A comparative experimental study of these three systems is thus ideally suited for understanding the role of dissipation in weak-field CC.

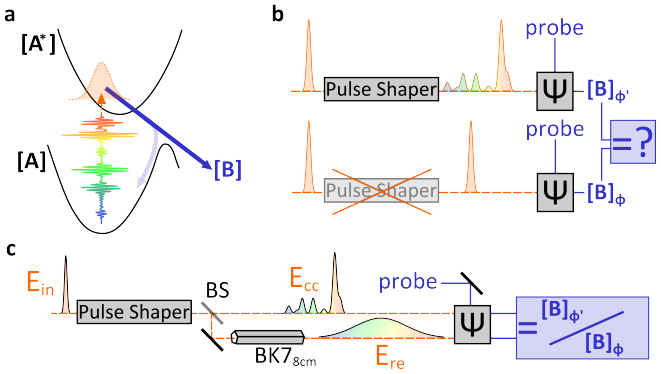

Figure 1: Concept and experimental realisation of self-referenced weak-field coherent control. (a) A specifically designed electric field photoexcites a molecular system from its ground [A] to an excited electronic state [A*] and changes the photoproduct yield, [B], compared to a transform-limited excitation pulse. (b) Common experimental implementation of feedback-loop guided coherent control. Ψ is the quantum system under study, $[B]_{\phi'}$ and $[B]_{\phi}$ the photoproduct yields for shaped and unshaped pulses, respectively. (c) Referenced coherent control approach used in this study. An initially transform-limited pulse (E_{in}) is shaped by a spatial light modulator (SLM) operated in a double pass (8f) geometry and then split into two identical copies with a 50:50 beamsplitter (BS). One copy (E_{cc}) travels directly to the sample, while the other (E_{re}) is strongly chirped by passing through an 8 cm BK7 glass rod. The ratio of simultaneously performed, but individual, experiments with the chirped and the unchirped pulse reveals the degree of achievable phase-dependent coherent control.

The experimental procedures for performing CC have been presented in detail previously [15]. They often involve a spatial light modulator to generate the complex electric control field from a transform-limited ultrashort laser pulse (Fig. 1b) [23]. The shaped pulse photoexcites the molecular system of interest followed by a time-delayed probe pulse. The resulting transient absorbance reports on the control target, such as photoproduct formation. Comparing the product yield to that obtained with a transform-limited pulse reveals the amount of achievable control. A feedback-loop guided search algorithm determines the optimal control field as the underlying molecular potential energy surface is rarely known [24]. Accessing the largest possible search space requires arbitrary waveforms, which is only achievable by manipulating both the phase and the amplitude of the electric field. Amplitude modulation, however, requires renormalisation of the control result for the excitation probability given by the overlap integral between the molecular absorption cross-section and the altered spectrum of the shaped excitation pulse [15]. A major experimental challenge is the elimination of artefacts in the feedback-loop optimisation. Since the algorithm is blind to the process of interest and usually only records pulse spectra or intensities, any experimental imperfection can lead to signatures that resemble a control scenario, but in fact result from trivial effects such as slight spectral miscalibrations, spatial beam inhomogeneities or beam displacements caused by spatio-temporal coupling, for example [25].

Results

We implement an intrinsically self referenced experimental approach to weak-field CC (Figure 1c), which we found to be minimally artefact prone as it eliminates the need for computational

renormalisation. A spatial light modulator operated in a double-pass geometry to minimise spatio-temporal coupling (Supplementary Information S1) [25], amplitude and phase shapes an initially transform-limited pump pulse with a typical duration of 10-20 fs. The resulting pulse is split into two identical copies with a 50:50 broadband beamsplitter. One copy, the control pulse, interacts with the sample and a time-delayed probe pulse evaluates the degree of control by recording the transient absorbance of the sample. We chirp the second pulse copy to ~2 ps by passing it through a long glass rod and measure the photoproduct absorbance analogously. The degree of control is given by the ratio of these simultaneously performed experiments (Supplementary Information S2).

In contrast to most previous implementations of CC, we do not compare the product yield to a transform-limited, but instead to a strongly chirped pulse. Whether a linearly chirped pulse reproduces the yield obtained with a transform-limited pulse is irrelevant; our experiment asks whether a specifically shaped pulse can achieve a different outcome than a strongly chirped one. If the latter produces no control, the result is identical to using a transform-limited pulse as a reference. If it does, then we simply investigate how different the achievable control is with a specifically shaped over a strongly chirped pulse. In any case, our experiment asks the question whether a specific spectro-temporally shaped electric field can achieve a different outcome than another - chirped and amplitude shaped - field, which is the essence of CC (Supplementary Information S3).

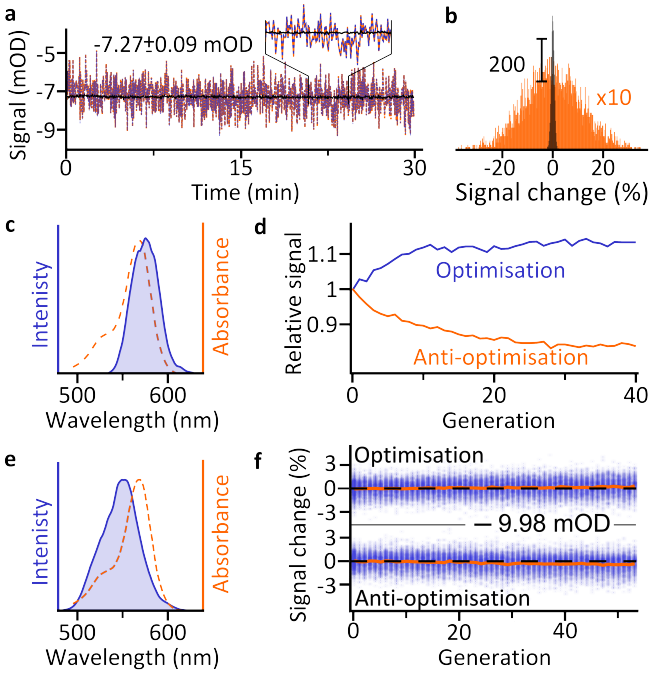

Figure 2: Self-referenced coherent control of rhodamine 101 under high and weak-field conditions. (a) Stimulated emission (620 – 680 nm) signal magnitudes measured for the shaped (blue, dashed) as well as the shaped and additionally chirped (orange, dashed) pump pulses in comparison to their ratio (black). The pulse spectrum is modulated randomly as described in the methods, but no feedback loop is implemented. (b) Histograms for the relative fluctuations in the referenced (black) and the absolute signal (orange, incidences multiplied by 10 for clarity). (c) Rhodamine 101 absorption spectrum (dashed) and high-field excitation pulse spectrum (solid). (d) Optimisation and anti-optimisation experiments performed on rhodamine 101 under high-field conditions show convergence after approximately 20 generations. Both experiments are normalised with respect to

their respective mean signal of the first generation. (d) Rhodamine 101 absorption spectrum (dashed) and weak-field excitation pulse spectrum (solid). (e) Optimisation and anti-optimisation experiments performed on rhodamine 101 under weak-field conditions fail to identify optimal or anti-optimal pulse shapes. All fitness values recorded in a total of 56 experiments (28 optimisation and anti-optimisation) are included in the figure (blue dots), the mean value of each generation is indicated by the orange line.

We benchmark the performance of our referencing approach by simultaneously measuring the transient stimulated emission (SE) of rhodamine 101 (optical density, OD = 0.7) in both signal and reference channels at low excitation levels (-7.27 mOD SE signal corresponds to ~1 % of all molecules excited). Non feedback-loop guided random spectral amplitude shaping induces strong SE signal fluctuations (±20 % of the signal), which are efficiently suppressed in the normalised signal ratio (Figure 2a). A histogram representation reveals a Poissonian distribution as expected for a shot-noise limited process with residual fluctuations on the order of 1.2% of the SE signal (-7.27 ±0.09 mOD at 95% confidence interval) with no detectable drift in 30 min, comparable to the time scale of a feedback-loop guided control experiment (Figure 2b). To demonstrate that our referenced CC experiment is capable of maximising or minimising a control target, we study the population transfer from the ground to the excited electronic state of rhodamine 101 under high-field conditions. Phase-only shaping of an initially 16 fs pulse (Figure 2c) allows us to achieve a contrast of ~30% between optimisation and anti-optimisation experiments within 20 generations. The additional 8 cm of BK7 in the reference pump arm adds approximately 5600 fs^2 of group delay dispersion. Under such referencing conditions both optimisation and anti-optimisation of the excitation probability is possible, in agreement with previous reports [26].

Following these proof-of-principle experiments, we attempt feedback loop guided weak-field CC on rhodamine 101. The initial excitation pulse (11.5 fs transform-limit) is chosen such that it fully overlaps with all major vibronic transitions of the rhodamine 101 absorption spectrum (Figure 2e), rather than the experimentally advantageous partial overlap for the high-field experiment [26], but remark that the genetic algorithm is in principle capable of re-establishing a pulse spectrum comparable to the high-field excitation pulse. We perform a total of 56 experiments at a stimulated emission signal of -9.98 mOD (exciting 1.5% of molecules in the excitation volume) and evaluate the degree of CC as the ratio between signal and reference channel at a pump-probe delay of 30 ps (Figure 2f). We find no evidence for weak-field CC in agreement with recent results obtained for single terrylene molecules [27]. The slight deviation of the generation mean from zero (0.2% for the optimisation and -0.4% for the anti-optimisation experiments after 50 generations) is likely caused by difficulties associated with perfectly referencing two signal channels [28], especially in the presence of a feedback-loop guided search algorithm capable of optimising for any imperfection in the normalisation (Supplementary Information S4).

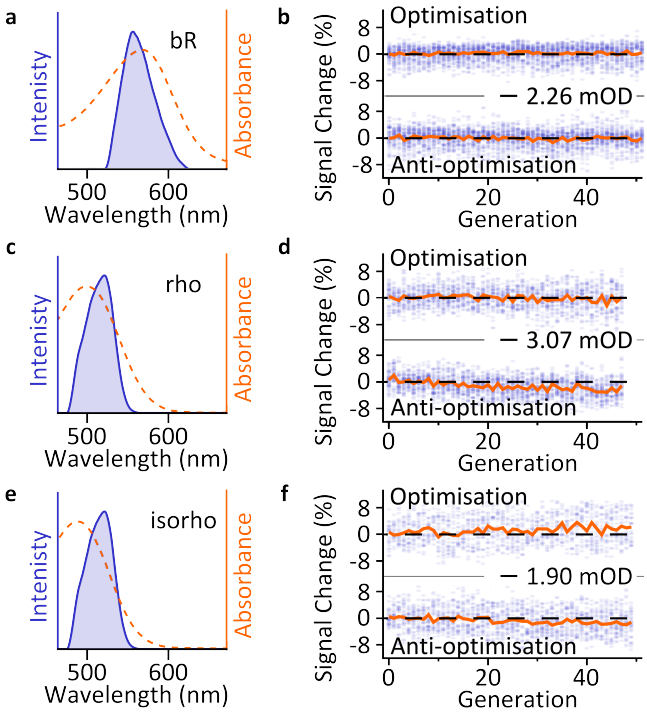

Figure 3: Weak-field coherent control on retinal protonated Schiff base embedded in different opsin proteins. (a,c,e) Excitation pulse (solid, blue) and absorption spectra (orange, dashed) for bacteriorhodopsin (bR), rhodopsin (rho) and isorhodopsin (isorho) respectively. (b,d,f) Optimisation and anti-optimisation experiments performed on bR, rho and isorho, respectively. Individual fitness values (blue dots) are shown together with the mean performance (orange line). The black dashed line represents the original signal value. All CC experiments are performed at a pump-probe delay of 30 ps, which is more than an order of magnitude longer than the vibrational dephasing times of photoexcitation induced vibrational wavepackets in these systems, as well as the completion time for the primary photoisomerisation events [29,30].

The robustness of our approach to artefact-induced feedback-loop convergence, as verified by further control experiments using glass rods (Supplementary Information S2), allows us to move towards systems where weak-field CC has been reported and predicted to be possible [10]. We use a 14.4 fs excitation pulse resonant with the absorption spectrum of bR (Figure 3a) at a signal level measured at the maximum of the photoinduced absorption of ~2.3 mOD, which corresponds to only 1.3 out of 100 molecules interacting with a second photon. After performing 20 CC experiments (10 optimisation, 10 anti-optimisation) on bR, we find no evidence for weak-field CC (3b), despite the standard deviation of the control signal (1.9%) being comparable to previous reports [13].

We repeated these experiments with rho, where the isomerisation proceeds much more rapidly than in bR, but with an almost identical quantum efficiency. Due to the limited compression range of our chirped mirrors, the 13 fs excitation pulse spectrum is restricted to wavelengths longer than 485 nm and the spectral overlap with the absorption spectrum is hence less ideal than for bR (Figure 3c). It is nevertheless possible to generate vibrational wavepackets in almost all degrees of freedom by employing this excitation pulse [29], as expected from the large homogeneous broadening of the system [31]. We adjusted the incident photon flux to reach a signal magnitude at the maximum of the photoinduced absorption of ~3.1 mOD (a calculated 1.1 photons absorbed per 100 molecules) and perform a total of 10 weak-field CC experiments (5 optimisation, 5 anti-optimisation). As previously, we observe no shaping convergence beyond the error of the measurement (Figure 3d), a result that

is repeated for isorho (Figure 3e,f). The standard deviation of the control signals of 3.0 and 3.9% for rho and isorho were slightly higher than for bR, due to increased sample scatter.

Discussion

The experiments presented on all four systems reported here fail to identify optimal or anti-optimal pulse shapes exhibiting CC in the strict one-photon limit. Especially in the case of rhodamine 101 and bR we relied on excitation fields that cover all major vibronic transitions of the absorption spectra ruling out insufficient bandwidth as the reason for our observations. Even for rho and isorho, where the overlap is less optimal, our excitation bandwidths exceed those used in previous reports [13,15,16,32] and are thus unlikely to be responsible for the lack of control. In the case of rhodamine 101 we found no evidence for weak-field CC, which, at our extremely low signal levels, is in good agreement with previous reports [15,27]. Importantly, small but still measurable feedback-loop convergence of the generation mean (0.2% for the optimisation, –0.4% for the anti-optimisation) as also observed for rho and isorho (Figure 3d,f) excludes the possibility that our failure to identify considerable weak-field control is a result of insufficient experimental sensitivity.

The lack of observable CC in this study contrasts with previous reports [13,15] and most likely stems from an optimised experimental setup in terms of suppression of potential measurement errors that could be exploited by a genetic algorithm. These include (i) a calibration-free compensation of changes in the excitation efficiency caused by amplitude shaping and (ii) confident operation in the one-photon limit. The latter point is especially important when dealing with systems such as bR where low signal levels are partially caused by considerable overlap between photobleach and photoproduct spectra, which have opposite signs in the differential absorbance measurement. As a result, previous experiments[13] may have accidentally been operating at excitation levels with two-photon interaction probabilities on the order of the reported phase-only weak-field CC levels (Supplementary Information S5).

The referencing approach implemented here is of particular relevance for weak-field control given that theoretical treatments have explicitly employed linearly chirped pulses [11,12]. It should have enabled us to reveal any weak-field CC down to the few percent level, which is affected by the arrival times of different spectral components within the temporal envelope of the electric control field. In order to be consistent with our observations, control fields identifiable by different referencing approaches but invisible to ours would therefore have to be independent of linear chirp, that is, independent of the temporal duration of the temporal envelope. Such an observation, however, would be inconsistent with the general concept of the interference of specifically tailored vibronic wavepackets, which evolve on the femtosecond timescale.

In contrast to previous work[15,33] our results suggest that weak-field CC in the condensed phase at ambient condition is difficult to achieve, if not impossible. We find no evidence for weak-field CC, irrespective of the excited state properties of the system under study even though the degrees of control predicted by theory (~20 %) [12] should have been readily revealed by our experiments. A possible explanation of our results that is consistent with the current theoretical treatments is that the critical dissipation timescale for weak-field CC is in fact electronic dephasing, which takes place on the few tens of femtoseconds timescale, rather than excited state decay, which has been used previously [11,12] and takes hundreds of femtoseconds or longer. Another, more drastic explanation, could be that currently available theoretical treatments fail to correctly describe the molecular dynamics of a complicated molecular system or its initial interaction with a complex electric excitation field. What the further implications are for the importance and meaning of quantum effects under natural, weak-field illumination demands for further theoretical studies, but promises

to be exceptionally informative for our understanding of the coherent interaction between light and matter at the single photon level.

Methods

Genetic Algorithm and pulse shaping

We rely on a genetic algorithm based on the *Genetic Algorithm Toolbox* (Department of Automatic Control and Systems Engineering of The University of Sheffield, UK), which has been successfully employed in previous CC experiments [15]. All shaping experiments are performed with a zero-dispersion 4f grating stretcher operated in double-pass geometry to avoid spatio-temporal coupling with a spatial light modulator (Jenoptik SLMS320d) in the Fourier plane. To facilitate algorithm convergence we do not optimise every spatial light modulator pixel individually but employ a reduced number of phase and amplitude parameters covering the full pulse bandwidth and interpolate over the entire pixel mask. Additionally, we parametrise our shaping space at 6 bit and allow the wavelength-dependent amplitude and phase parameters to vary freely within the set boundaries.

Each generation is evaluated against the control target and 50% of the individuals are selected, based on their fitness values, for breeding by stochastic undersampling. The chromosomes of these survivors are used as a gene-pool for the following generation. We exchange bits between chromosomes (gene crossover at a 70% probability per chromosome) and randomly swap bits (mutation at a 60% probability per chromosome) to generate new individuals for the next generation. The newly generated individuals are combined with the survivors of the previous generation to form the second generation and the control target is re-evaluated. This process is repeated for a pre-selected number of generations.

To account for slight imperfections in the referencing as for example caused by the 50:50 beamsplitter with wavelength dependent reflectivities between 49-51%, we renormalise the fitness value of each individual to the value obtained by pure amplitude shaping.

Shaping experiments on rhodamine 101

Initial benchmark experiments on rhodamine 101 (Figure 2a,b): 16 fs pulse (2.3 nJ) centered at 576 nm with a pump focus of 82 µm and a probe focus of 48 µm diameter (FWHM), respectively. We evaluate the stimulated emission signal in the 620-680 nm spectral region at a pump-probe time delay of 30 ps while modulating the wavelength-dependent pump amplitude. Each signal is integrated for 100 ms at a laser repetition rate of 10 kHz. A 200 µm flow-cell is used.

High-field CC on rhodamine 101 (Figure 2c,d): The pump power is set to 165 nJ and pump and probe foci are adjusted to 78 µm and 47 µm diameter (FWHM), respectively. The amplitude is kept constant and the phase is varied within -2π; 2π with a total of 30 parameters over the 530-610 nm spectral range. The CC experiment is performed over 40 generations consisting of 50 individuals. The signal is evaluated in the 620-680 nm spectral region of the SE signal at a pump-probe time delay of 30 ps. Each signal is integrated for 100 ms at a laser repetition rate of 10 kHz.

Weak-field CC on rhodamine 101 (Figure 2e,f): The pump power is set to 2.2 nJ and pump and probe foci diameter (FWHM) are adjusted to 70x75 µm and 50 µm, respectively. The amplitude is varied freely (0; 1) whereas the phase shaping space is set to either $(-2\pi; 2\pi)$ or $(-4\pi; 4\pi)$ with the latter

ensuring that potential limitations due to imperfect phase wrapping are detected. A moderately constant excitation level is ensured (within ±5%) by renormalising the randomly generated pulse shapes for their theoretical excitation efficiency calculated as the overlap integral with the linear absorption spectrum (Supplementary Information S6). We perform experiments with 32 or 50 phase and amplitude variables over the 490-605 nm spectral range. Each CC experiment is performed over 55 generations consisting of 50 individuals, respectively. The signal is evaluated in the 620-680 nm spectral region of the SE signal at a pump-probe time delay of 30 ps. Each signal is integrated for 100 ms at a laser repetition rate of 10 kHz. The standard deviation of the 9.98 mOD optimisation signal over the period of all experiments was determined to being 0.5% or ±50 μOD.

Shaping experiments on proteins

All experiments are performed at a laser repetition rate of 2 kHz in order to reduce protein damage caused by flow induced shear while ensuring fresh protein sample at each laser shot. Signals larger than ±12% are re-evaluated during the experiment to exclude artefacts induced by sample scattering. The integration time for evaluating each individual pulse shape is increased from 100 ms to 1 s in order to account for the reduced signal-to-noise ratio due to both the five times lower repetition rate of 2 kHz as well as scattering-induced measurement noise. A 500 μm flow-cell is used.

Weak-field CC on bR (Figure 3a,b): bR suspended in MilliQ water at an OD of 0.49 per pathlength is light-adapted prior to each experiment and kept in its light-adapted form by a halogen lamp equipped with UV and IR filter (wavelength range: 495-900 nm, FGS900S and FGL495S both Thorlabs) and excited with 1.8 nJ of pump power. The CC signal is evaluated from the photoproduct signal in the 620-700 nm spectral region at a pump-probe delay of 30 ps. We employ a total of 66 shaping parameters (33 phase and amplitude) over the 520-620 nm shaping range. Each generation consists of 30 individuals and the shaping space is set to (0; 1) for amplitude and (-2π; 2π) for the phase values. A total of 20 (10 optimisation and anti-optimisation) experiments is performed. Pump and probe foci are adjusted to 63x67 μm and 43 μm diameter (FWHM), respectively. A constant excitation level is ensured (within ±5 %) by renormalising the randomly generated pulse shapes for their theoretical excitation efficiency calculated as the overlap integral with the linear absorption spectrum. The standard deviation of the 2.26 mOD optimisation signal over the period of all experiments was determined to being 1.9 % or ±43 μOD which is comparable to previous reports [13].

Weak-field CC on rho (Figure 3c,d): rho is suspended in Ammonyx LO at an OD of 0.45 per pathlength and excited with 2.5 nJ of pump power. Prior to the experiments we added 2 mM hydroxylamine to the suspension to remove isomerised retinal chromophores from the protein pockets. The CC performance is evaluated at a pump-probe delay of 30 ps in the 585-635 nm spectral region of the photoproduct signal. We employ a total of 50 shaping parameters (25 phase and amplitude) over the 480-545 nm shaping range. Each generation consists of 30 individuals and the shaping space is set to (0; 1) for amplitude and (-2π; 2π) for the phase values. A total of 10 (5 optimisation and anti-optimisation) experiments are performed. Pump and probe foci are adjusted to 61x75 μm and 40 μm diameter (FWHM), respectively. A constant excitation level is ensured (within ±5 %) by renormalising the randomly generated pulse shapes for their theoretical excitation efficiency calculated as the overlap integral with the linear absorption spectrum. The standard deviation of the 3.07 mOD optimisation signal over the period of all experiments was determined to being 3.0% or ±92 μOD.

Weak-field CC on isorho (Figure 3e,f): Analogous to rho but at an OD of 0.39 and a pump power of 4.4 nJ. A total of 6 (3 optimisation and anti-optimisation) experiments is performed. The standard deviation of the 1.90 mOD optimisation signal over the period of all experiments was determined to being 3.9% or ±74 µOD.

After completion of the experiments both rho and isorho were fully photobleached by exposure to ambient light to verify that the retinal protonated Schiff base chromophore was successfully removed from the protein pocket.

Estimating photons per molecule

Based on the pump diameters at *1/e* and the carrier wavelength of the respective pump pulse we compute the number of photons per pulse and unit area. The fraction of photons absorbed is directly determined from the measured absorption and pump spectra and the optical density. The ratio of absorbed photons to the amount of molecules in the same unit area, as estimated from the optical density and the molar absorption coefficients ε_{RHO101}=90000, ε_{bR}=54000, ε_{isorho}=40600 and ε_{rho}=40600 $M^{-1}cm^{-1}$ at the absorption maximum) yields an estimate of the absorption probability per molecule. The pump foci are assumed as being symmetrical Gaussians with FWHM diameters of d_{RHO101}=65 µm, d_{bR}=65 µm, d_{isorho}=70 µm and d_{rho}=70 µm for simplicity. In all experiments presented here we estimate excitation densities of <2 photons per 100 molecules.

Acknowledgments

We would like to thank Katelyn M. Spillane, Giovanni Bassolino, Garrick F. Taylor and Anthony Watts for the rhodopsin, isorhodopsin and bacteriorhodopsin samples. P.K. proposed the project, P.K. and M.L. designed the experiment, M.L. performed the experiment, P.K. and M.L. analysed and discussed the data and wrote the manuscript together.

1. Tannor, D. J. & Rice, S. A. Control of selectivity of chemical reaction via control of wave packet evolution. *J. Chem. Phys.* **83,** 5013–5018 (1985).

2. Brumer, P. & Shapiro, M. Control of unimolecular reactions using coherent light. *Chem. Phys. Lett.* **126,** 541–546 (1986).

3. Brumer, P. & Shapiro, M. Laser control of molecular processes. *Annu. Rev. Phys. Chem.* **43,** 257–282 (1992).

4. Warren, W. S., Rabitz, H. & Dahleh, M. Coherent control of quantum dynamics: the dream is alive. *Science* **259,** 1581–1589 (1993).

5. Gordon, R. J. & Rice, S. A. Active control of the dynamics of atoms and molecules. *Annu. Rev. Phys. Chem.* **48,** 601–641 (1997).

6. Rabitz, H., de Vivie-Riedle, R., Motzkus, M. & Kompa, K. Whither the Future of Controlling Quantum Phenomena? *Science* **288,** 824–828 (2000).

7. Shapiro, M. & Brumer, P. *Principles of the Quantum Control of Atomic and Molecular Processes*. (Wiley, New York, 2003). doi:10.1109/74.370583

8. Brif, C., Chakrabarti, R. & Rabitz, H. Control of quantum phenomena: past, present and

future. *New J. Phys.* **12,** 075008(R) (2010).

9. Brumer, P. & Shapiro, M. One photon mode selective control of reactions by rapid or shaped laser pulses: An emperor without clothes? *Chem. Phys.* **139,** 221–228 (1989).

10. Spanner, M., Arango, C. A. & Brumer, P. Communication: Conditions for one-photon coherent phase control in isolated and open quantum systems. *J. Chem. Phys* **133,** 151101(R) (2010).

11. Katz, G., Ratner, M. A. & Kosloff, R. Control by decoherence: weak field control of an excited state objective. *New J. Phys.* **12,** 015003(R) (2010).

12. Arango, C. A. & Brumer, P. Communication: One-photon phase control of cis-trans isomerization in retinal. *J. Chem. Phys.* **138,** 071104(R) (2013).

13. Prokhorenko, V. I. *et al.* Coherent control of retinal isomerization in bacteriorhodopsin. *Science* **313,** 1257–1261 (2006).

14. Hoki, K. & Brumer, P. Dissipation effects on laser control of cis/trans isomerization. *Chem. Phys. Lett.* **468,** 23–27 (2009).

15. Prokhorenko, V. I., Nagy, A. M. & Miller, R. J. D. Coherent control of the population transfer in complex solvated molecules at weak excitation. An experimental study. *J. Chem. Phys.* **122,** 184502(R) (2005).

16. van der Walle, P., Milder, M. T. W., Kuipers, L. & Herek, J. L. Quantum control experiment reveals solvation-induced decoherence. *Proc. Natl. Acad. Sci. USA* **106,** 7714–7717 (2009).

17. Mathies, R. A., Brito Cruz, C. H., Pollard, W. T. & Shank, C. V. Direct Observation of the Femtosecond Excited-State cis-trans Isomerization in Bacteriorhodopsin. *Science* **240,** 777–779 (1988).

18. Schoenlein, R. W., Peteanu, L. A., Mathies, R. A. & Shank, C. V. The First Step in Vision: Femtosecond Isomerization of Rhodopsin. *Science* **254,** 412–415 (1991).

19. Polli, D. *et al.* Wavepacket Splitting and Two-Pathway Deactivation in the Photoexcited Visual Pigment Isorhodopsin. *Angew. Chem. Int. Ed.* **53,** 2504–2507 (2014).

20. Tittor, J. & Oesterhelt, D. The quantum yield of bacteriorhodopsin. *FEBS Lett.* **263,** 269–273 (1990).

21. Kim, J. E., Tauber, M. J. & Mathies, R. A. Wavelength dependent cis-trans isomerization in vision. *Biochemistry* **40,** 13774–13778 (2001).

22. Schoenlein, R. W., Peteanu, L. A., Wang, Q., Mathies, R. A. & Shank, C. V. Femtosecond Dynamics of Cis-Trans Isomerization in a Visual Pigment Analog: Isorhodopsin. *J. Phys. Chem.* **97,** 12087–12092 (1993).

23. Weiner, A. M., Leaird, D. E., Wiederrecht, G. P. & Nelson, K. A. Femtosecond pulse sequences used for optical manipulation of molecular motion. *Science* **247,** 1317–9 (1990).

24. Rabitz, H. A., Hsieh, M. M. & Rosenthal, C. M. Quantum optimally controlled transition landscapes. *Science* **303,** 1998–2001 (2004).

25. Brinks, D., Hildner, R., Stefani, F. D. & van Hulst, N. F. Beating spatio-temporal coupling: implications for pulse shaping and coherent control experiments. *Opt. Express* **19,** 26486–26499 (2011).

26. Cerullo, G., Bardeen, C. J., Wang, Q. & Shank, C. V. High-power femtosecond chirped pulse excitation of molecules in solution. *Chem. Phys. Lett.* **262,** 362–368 (1996).

27. Weigel, A., Sebesta, A. & Kukura, P. Shaped and Feedback-Controlled Excitation of Single Molecules in the Weak-Field Limit. *J. Phys. Chem. Lett.* **6,** 4023–4037 (2015).

28. Dobryakov, A. L. *et al.* Femtosecond pump/supercontinuum-probe spectroscopy: optimized setup and signal analysis for single-shot spectral referencing. *Rev. Sci. Instrum.* **81,** 113106(R) (2010).

29. Schnedermann, C., Liebel, M. & Kukura, P. Mode-Specificity of Vibrationally Coherent Internal Conversion in Rhodopsin During the Primary Visual Event. *J. Am. Chem. Soc.* **137,** 2886–2891 (2015).

30. Liebel, M. *et al.* Direct Observation of the Coherent Nuclear Response after the Absorption of a Photon. *Phys. Rev. Lett.* **112,** 238301(R) (2014).

31. Myers, A. B., Harris, R. A. & Mathies, R. A. Resonance Raman excitation profiles of bacteriorhodopsin. *J. Chem. Phys.* **79,** 603–613 (1983).

32. Florean, A. C. *et al.* Control of retinal isomerization in bacteriorhodopsin in the high-intensity regime. *P. Natl. Acad. Sci. USA* **106,** 10896–10900 (2009).

33. Prokhorenko, V. I. *et al.* Response to Comment on 'Coherent Control of Retinal Isomerization in Bacteriorhodopsin'. *Science* **317,** 453c (2007).